Research Article

Ligang Zhang*, Xiao Fei Fu, G. R. Liu, Shi Bin Li, Wei Li, and Sining Qu

Models for evaluating craters morphology, relation of indentation hardness and uniaxial compressive strength via a flat-end indenter

https://doi.org/10.1515/geo-2018-0022
Received Nov 27, 2017; accepted Apr 26, 2018

Abstract: In this work, the intensive theoretical study and laboratory tests are conducted to evaluate the craters morphology via the flat-ended indenter test, relationship of indentation hardness (HRI) and uniaxial compressive strength (UCS). Based on the stress distribution, failure process and Mohr–Coulomb failure criterion, the mathematical mechanical models are presented to express the formation conditions of "pulverized zone" and "volume break". Moreover, a set of equations relating the depth and apex angle of craters, the ratio of indentation hardness and uniaxial compressive strength, the angle of internal friction and Poisson's ratio are obtained. The depth, apex angle of craters and ratio of indentation hardness and uniaxial compressive strength are all affected by the angle of internal friction and Poisson's ratio. The proposed models are also verified by experiments of rock samples which are cored from Da Qing oilfield, the percentage error between the test and calculated results for depth, apex angle of craters and the ratio of HRI and UCS are mainly in the range of –1.41%–8.92%, –5.91%–3.94% and –8.22%–13.22% respectively for siltstone, volcanic tuff, volcanic breccia, shale, sand stone and glutenite except mudstone, which demonstrates that our proposed models are robust and effective for brittle rock.

Keywords: flat-end indenter; crater; indentation hardness (HRI); uniaxial compressive strength (UCS); brittle rock; Mohr–Coulomb failure criterion; angle of internal friction; Poisson's ratio

1 Introduction

Rock hardness is a measure of the resistance to localized plastic deformation induced by either mechanical indentation or abrasion. There are three main types of hardness measurements: scratch [1, 2], rebound [3–5], and indentation [6]. Within each of these classes of measurement there are individual measurement scales. In drilling engineering, the interface of rock and bit interface process is very complex. In order to describe the rock failure and mechanism, many scholars usually select a simplified indention test using flat-end indenter [7–9], and the indentation hardness is also usually used to assess the drillability of rocks [10, 11]. For decades, many scholars have made helpful theoretical and experimental contributions to studies on the indentation process and rock break mechanism. The important experimental phenomena and conclusions have been established by Yu [12], Cheatman [13], Xia [14], Yang [15] and Xu [16] as follows, 1) there is a "pulverized zone"under the indenter. The pulverized zone has a spherical or conical shape, and is formed by local crushing under a high pressure. 2) The jump phenomenon was appearing in the indentation process. It means that the invasion depth increases in uniformity with the increase of load at the beginning, while the load reaches a certain critical value, the fragment rock will be jumped from the surrounding rock, the load falls temporarily and the invasion depth increases sharply. Then, the indenter continues indenting to a new depth. 3) The apex angles of crater were mainly distributed in 120 ~ 150°. Uniaxial compressive strength (UCS) is the capacity of rock to withstand compressive loads, which is widely used for estimating the mechanical properties of rock material in rock engineering projects [17–19]. The UCS is usually established using standardized laboratory tests as set forth by the International

***Corresponding Author: Ligang Zhang:** Department pf Petroleum Engineering, Northeast Petroleum University, Daqing 163318, Heilongjiang, China; Department of Aerospace Engineering and Engineering Mechanics, University of Cincinnati, Ohio, United States of America; Email: zhangligang529@163.com
Xiao Fei Fu, Shi Bin Li, Wei Li, Sining Qu: Department pf Petroleum Engineering, Northeast Petroleum University, Daqing 163318, Heilongjiang, China
G. R. Liu: Summer Part-Time Professor, School of Mechanical Engineering, Hebei University of Technology, Tianjin, China; Department of Aerospace Engineering and Engineering Mechanics, University of Cincinnati, Ohio, United States of America

Society for Rock Mechanics and American Society for Testing and Materials [20], which requires a careful test set-up and time consuming [21, 22]. In order to overcome many of the problems associated with the unconfined compression test, repeating research attempts are trying to predict UCS through the more rapid hardness testing methods. Correlation equations between hardness and UCS have been established through statistical and regression analysis of experiment results, such as indicated by Broch and Franklin [23], Sheorey *et al.* [24], Sachpazis [25], Tug˘rul and Zarif [26], Shalabi *et al.* [27] and Wang [28] have revealed the schmidt hammer rebound value is well correlated with UCS for volcanic rocks, coal, carbonate rocks, granites and shales. This research focuses on the analyses of rock failure process mechanisms of indentation via a flat-ended indenter, and aims to establish theoretical models for the craters morphology, the indentation hardness (HRI) with flat-ended indenter as a predictor of the UCS for brittle rocks.

2 Indentation hardness tests

The typical indentation hardness testing device is shown in Figur 1.

The material of the indenter is usually high-strength steel after heat treatment, and the hardness should be 60~62 HRC. The head of indenter may be a cylinder whose diameter ranges from 2mm to 5mm for testing different hard rocks. The indentation hardness (HRI) is defined as the pressure when the rock first break and can be expressed as follows [29].

$$\mathrm{HRI} = \frac{F_{\mathrm{st}}}{\pi a^2} \tag{1}$$

Where F_{st} is the force of the rock fails, and a is the radius of the indenter.

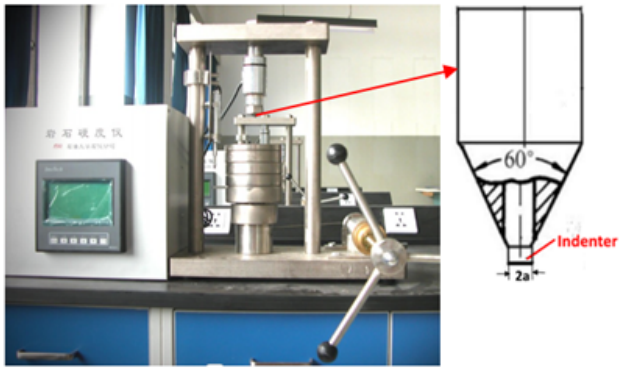

Figure 1: The typical indentation hardness testing device.

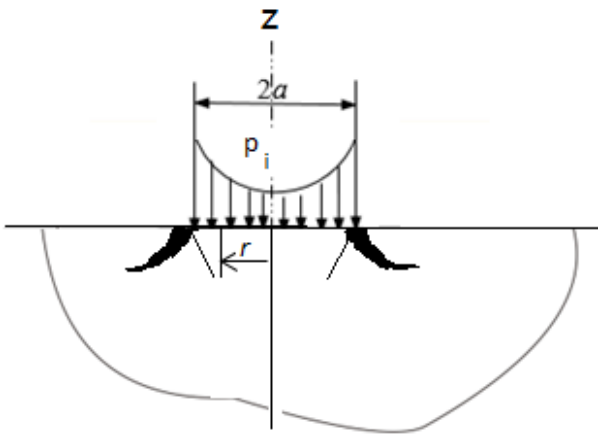

Figure 2: Distribution of pressure under indenter when initial contact.

With respect to the the solid linear elasticity, according to the theory of Hertz, the distribution of pressure under the indenter is given by

$$p_i = \frac{F}{2\pi a\sqrt{(a^2 - r^2)}} \tag{2}$$

Where p_i is the pressure on the surface of the solid (rock); F is the external force exerting on the indenter.

The pressure distribution is plotted in Figure 3 with r is the distance from calculated point to Z axis. The pressure is not uniform, and the value reaches the maximum at the edge and the minimum value at the center. Because the maximum pressure is at the edge of indenter, the first group cracks appear around the indenter edge.

The phenomenon is originally studied by Hertz, and the cracks are called as Hertz cracks [30]. With the plastic deformation or fracture produced on the edge of the contact area, the distribution of pressure is gradually becoming uniformly distributed. Then, the distribution of the pressure is homogenized as:

$$p = \frac{F}{\pi a^2} \tag{3}$$

The stress in the rock under indenter is the problem of an elastic half-space subjected to a pressure acting on the surface. The formulae were given by Cerruti [31] and Boussinesq [32]. The axial stress, circumferential stress and radial stress in the cylindrical coordinate system are expressed in the following equations respectively,

$$\sigma_z = p\left[1 - \left(\frac{z}{\sqrt{a^2 + z^2}}\right)^3\right] \tag{4a}$$

$$\sigma_r = \sigma_t = \frac{p}{2}\left[(1 - 2\mu) + \left(\frac{z}{\sqrt{a^2 + z^2}}\right)^3 - \frac{2(1+\mu)z}{\sqrt{a^2 + z^2}}\right] \tag{4b}$$

Where σ_z, σ_r and σ_t are axial stress, circumferential stress and radial stress, respectively, μ is Poisson's ratio, and z is the coordinate in z axis. The axial, circumferential and radial stresses along z axis are plotted in Figure 3. With the increase of distance from contact surface (the value of z), the axial stress, circumferential stress and radial stress are decreasing. The radial and circumferential stress decrease faster than the axis stress, which leads to an increase of the shear stress with the value of Z. When the shear stress reaches to the shear broken value at Z_0, it will generate the second group cracks at $Z_0$and extend to the surface. When the second group cracks meet the first group cracks, then a "pulverized zone" forms under the indenter as shown in Figure 4.

The"pulverized zone"is usually a bag, with a spherical or cone shape, which is formed by local crushing under a high pressure. The phenomenon has been studied by many researches [33–39]. With the increase of load, the"pulverized zone"pushes and extrudes to the parent rocks. When the shear stress reaches the shear broken value on one surface, the fragment will be jumped from the surrounding rock, and the volume broken occurs, as shown in Figure 5. Then, the indenter invades into the rock, with a jumping phenomenon occurring simultaneously, the load falls temporarily and the invasion depth increases sharply.

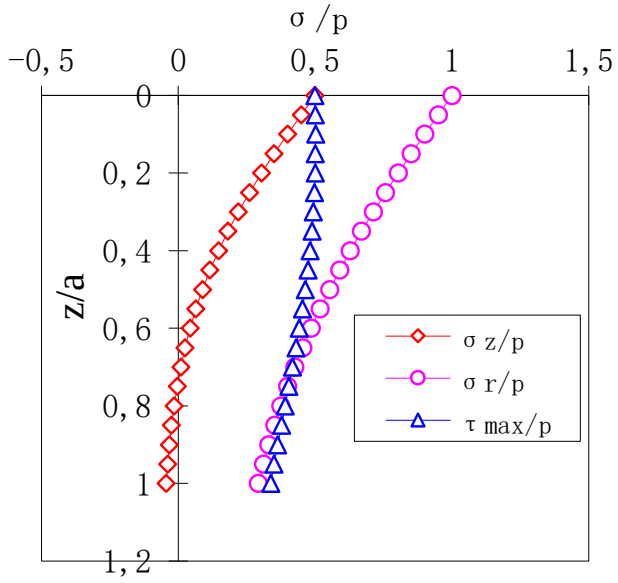

Figure 3: Distribution of stresses along Z axis.

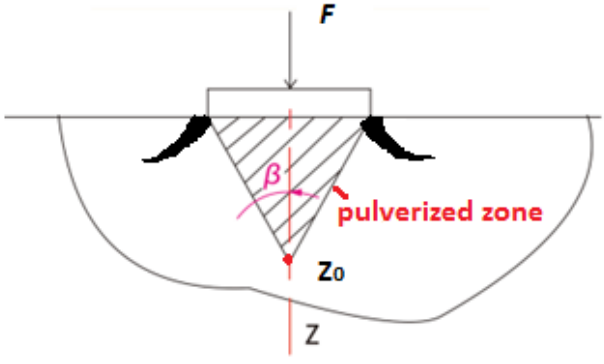

Figure 4: A pulverized zone formed beneath the indenter.

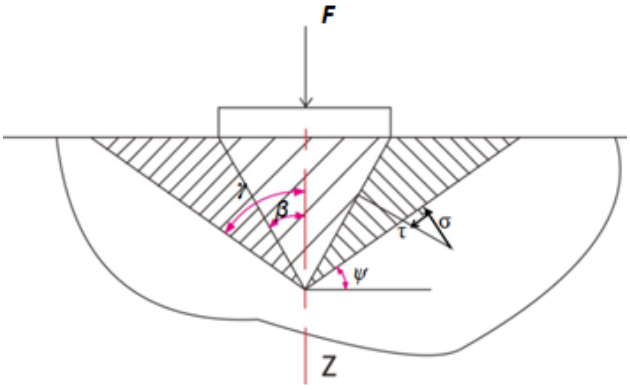

Figure 5: Volume break of rocks under the indenter.

3 Relationship between HRI and UCS

Many strength criterions have been proposed by various researchers, in all of them Mohr–Coulomb (MC) failure criterion is the most widely used for strength criterion [40–43]. It is a linear equation describing the conditions of material failure in the principal stress space. The expression is written as

$$\tau = \sigma \tan \varphi + c \tag{5a}$$

Where τ is shear stress; σ is normal stress; C is inherent shear strength; φ is the angle of internal friction.

It can also be written by the principal stresses as follows:

$$\sigma_1 = \sigma_3 \tan^2 \theta + UCS \tag{5b}$$

Where σ_1 is the first principal stress; σ_3 is the minimum principal stress; σ_c is the unconfined compress strength; $\theta = \frac{\pi}{4} + \frac{\varphi}{2}$.

In this paper, the MC criterion is used to describe rock failure. The following function F is used to determine the

easiest crush position along z axis:

$$F = \sigma_1 - \sigma_3 \tan^2\theta \tag{6}$$

The position which F reaches the maximum value is the easiest destroyed position. Substituting $\sigma_z = \sigma_1$, $\sigma_r = \sigma_3$ into Equation (6), Equation (6) becomes

$$F = p\left[1 - \left(\frac{z}{\sqrt{a^2+z^2}}\right)^3\right] - \frac{p}{2}\left[(1+2\mu) + \left(\frac{z}{\sqrt{a^2+z^2}}\right)^3 - \frac{2(1+\mu)z}{\sqrt{a^2+z^2}}\right]\tan^2\theta \tag{7}$$

Order $\frac{dF}{dz} = 0$, the maximum value of F is obtained, and the location of the second group cracks becomes:

$$z_o = a\sqrt{\frac{2(1+\mu)\tan^2\theta}{6+\tan^2\theta - 2\mu\tan^2\theta}} \tag{8}$$

Where Z_0 is the height of "pulverized zone".

The half apex angle β of the"pulverized zone"is shown as follows:

$$\beta = \operatorname{arccot}\left(\frac{z_0}{a}\right) \tag{9}$$

Where β is the half apex angle of "pulverized zone".

With the increase of load, the "pulverized zone"will transmit pressure to the parent rock, and the shear and normal stress at the arbitrary slope (as shown in Figure 5) of the parent rock can be calculated as follows:

$$\tau = \frac{p\cdot a}{L\cdot\sin\beta}\cos(\beta+\psi) \tag{10}$$

$$\sigma = \frac{p\cdot a}{L\cdot\sin\beta}\sin(\beta+\psi) \tag{11}$$

Where τ is the shear stress, σ is the normal stress, L is the length of slope, ψ is the angle of slope.

Substitute Equation (10), Equation (11) into Equation (4), it is obtained:

$$F = \tau - \sigma\tan\varphi = p\cdot\frac{a}{z_0}\frac{\sin\psi\cos(\beta+\psi+\varphi)}{\sin\beta\cos\varphi} \tag{12}$$

Let $\frac{dF}{d\psi} = 0$, the most easily destroyed angle of slope is gotten

$$\psi = \frac{\pi}{4} - \frac{\beta+\varphi}{2} \tag{13}$$

Substituting Equation (13) into Equation (5a) gives

$$\tau - \sigma\tan\varphi = \frac{p\cdot a}{z_o}\frac{\sin\psi\cos(\beta+\psi+\varphi)}{\sin\beta\cos\varphi} = C \tag{14}$$

When p satisfies Equation (15), the parent rock is broken under the shear stress and p is defined as indentation hardness.

$$p = \mathrm{HR}I \tag{15}$$

Substitute Equation (15) to Equation (14), we have

$$\mathrm{HRI}\cdot\frac{a}{z_o}\frac{\sin\left(\frac{\pi}{4}-\frac{\beta+\varphi}{2}\right)\cos\left(\frac{\pi}{4}+\frac{\beta+\varphi}{2}\right)}{\sin\beta\cos\varphi} = C \tag{16}$$

After trigonometric transformation, Equation (17) is obtained.

$$\mathrm{HRI}\cdot\frac{a}{z_o}\frac{1-\sin(\beta+\varphi)}{2\sin\beta\cos\varphi} = C \tag{17}$$

Solve Equation (17), multiple $\frac{10\sin\varphi}{10\sin\varphi}$, and the expression of HRI can be gotten as:

$$\mathrm{HRI} = \frac{Z_0}{a}\frac{2C\sin\beta\cos\varphi}{1-\sin(\beta+\varphi)}\left(\frac{1-\sin\varphi}{1-\sin\varphi}\right) \tag{18}$$

On the other hand, UCS can be expressed as

$$\mathrm{UCS} = \frac{2C\cos\varphi}{1-\sin\varphi} \tag{19}$$

The ratio of $\frac{\mathrm{HRI}}{\mathrm{UCS}}$ becomes

$$\frac{\mathrm{HRI}}{\mathrm{UCS}} = \frac{\sin\beta(1-\sin\varphi)}{1-\sin(\beta+\varphi)}\sqrt{\frac{2(1+u)\tan\theta^2}{6+\tan\theta^2-2\mu\tan\theta^2}} \tag{20}$$

The apex angle of the craters is shown as follows:

$$2\gamma = 2\left(\frac{\pi}{2}-\psi\right) = \frac{\pi}{2}+\beta+\varphi \tag{21}$$

Where γ is the half apex angle of craters.

4 The influence factors and laws

In Equation (8), (14) and (21), Z_0, γ and HRI/UCS can be expressed in Poisson ratio and internal friction angle. Therefore, the depthZ_0, the apex angle of craters 2γ, and HRI/UCS are affected only by Poisson ratio and internal friction angle. The changes of Z_0, 2γ and HRI/UCS are obtained in different values of Poisson ratio and internal friction angle, as shown in Figure 6a to Figure 6b.

Figure 6a shows the depth of craters increase as linearity function with the increase of the Poisson ratio. Figure 6b shows the depth of craters increase as exponential function with the increase of internal friction angle.

Figure 7a shows the apex angle of craters decrease as linearity function with the increase of the Poisson ratio. Figure 7b shows the depth of craters increase as linearity function with the increase of internal friction angle.

Figure 8a shows that, with the increase of the angle of Poisson's ratio, the ratio of HRI/UCS decreases as an exponential function. Figure 8b shows that, with the increase of internal friction angle, HRI/UCS is decreasing as an exponential function.

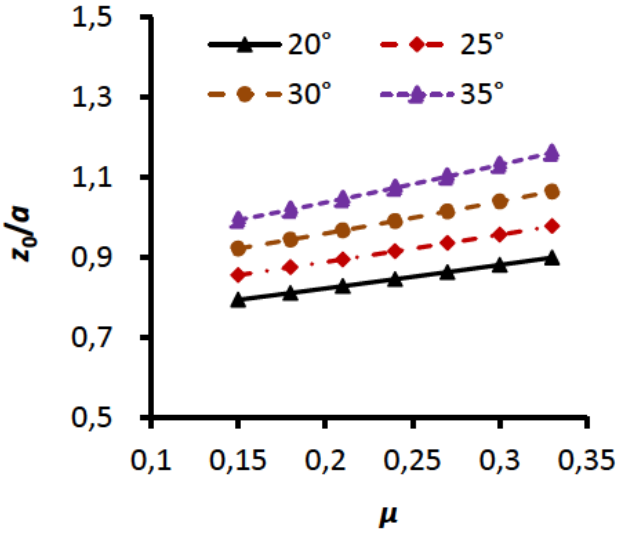

Figure 6a: Poisson's ratio effects on the ratio of z_0 and a in different Angle of internal friction.

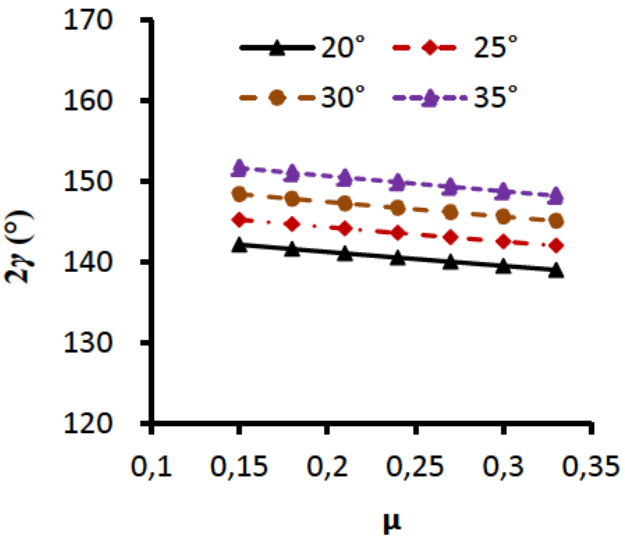

Figure 7a: Poisson's ratio effects on the apex angle of crater indifferent angle of internal friction.

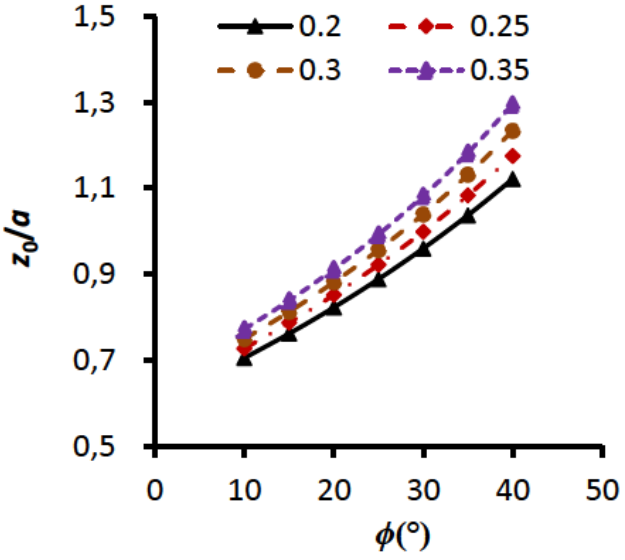

Figure 6b: Angle of internal friction effects on the ratio of z_0 and a in different Poisson's ratios.

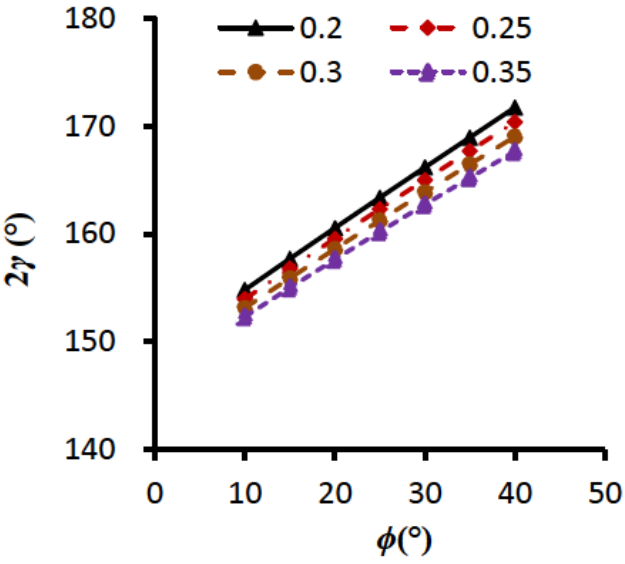

Figure 7b: Angle of internal friction effects on the apex angle of crater in different Poisson's ratios.

5 Experiment validation

In order to validate the present formulas and to assess its accuracy, the experiments are carried out to measure the indentation hardness and mechanical properties. Rock samples include Siltstone, Mudstone, volcanic tuff, volcanic breccia, shale, sand stone and glutenite are cored from Da Qing oilfield of china. The diameter of the indenter is 2mm. For avoiding the influence from the adjacent test point and the sample edge, the distance between two test points and the tests point to the edge are set bigger than 10mm. The test points and craters are shown in Figure 9. Three or more points are tested in each rock Sample.

After the indentation hardness experiments, cylindrical specimens with diameter of 25mm and a height-to-diameter ratio of 2 (±0.03) are cored, the UCS experiments are carried out. The mean test results include UCS, HRI, depth of craters, apex angle of craters and corresponding calculated results are listed in Table 1.

It can be clearly seen from Table 1, the percentage error between the test and calculated results for depth, apex angle of craters and the ratio of HRI and UCS are

Table 1: Comparison of the test and calculated results.

No.	lithology	UCS (MPa)	HRI (MPa)	Mean Z_0			Mean 2 γ			Mean HRI/UCS		
				Test (mm)	Calculation (mm)	Error (%)	Test (°)	Calculation (°)	Error (%)	Test (°)	Calculation (°)	Error (%)
1	Siltstone	71.33	1366.43	2.343	2.134	8.92	143.8	152.3	−5.91	19.16	21.24	10.86
2	Mudstone	30.46	368.58	2.647	2.051	22.52	116.5	144.2	−23.78	12.10	14.12	−16.69
3	Sand stone	22.35	342.39	2.264	2.121	6.32	145.4	148.9	−2.41	15.32	16.58	−8.22
4	Volcanic tuff	79.3	1844.13	2.487	2.522	−1.41	155.2	159.8	−2.96	23.25	24.15	3.87
5	Volcanic breccia	167.68	3184.13	2.404	2.369	1.46	153.3	156.4	−2.02	18.99	16.46	13.32
6	Shale	89.9	2023.66	2.127	1.988	6.54	154.2	148.4	3.76	22.51	23.44	4.13
7	Sand stone	17.98	320.34	2.434	2.359	3.08	149.8	152.1	−1.54	17.82	16.58	3.70
8	Sandstone	150.15	3158.6	2.351	2.235	4.93	157.6	153	2.92	21.04	21.07	−0.16
9	Sand stone	159.37	3169.9	1.987	2.068	−4.08	148.9	151.8	−1.95	19.89	19.52	1.86
10	Sand stone	128.1	1947.26	1.875	1.905	−1.60	145.4	148.9	−2.41	15.20	14.17	6.78
11	Glutenite	92.02	1598.43	2.273	2.137	5.98	154.7	151.5	2.07	17.37	17.79	−2.42
12	Sand stone	84.25	796.37	1.826	1.745	4.44	149.8	143.9	3.94	9.45	8.85	6.37

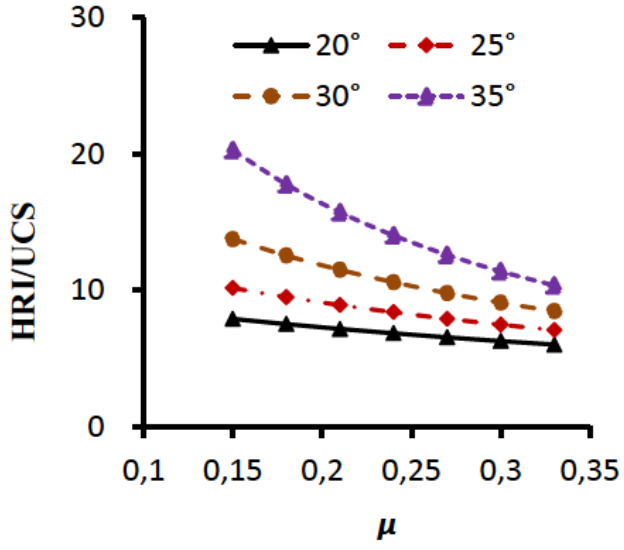

Figure 8a: Angle of internal friction effects on the ratio of HRI and UCS in different Poisson's ratios.

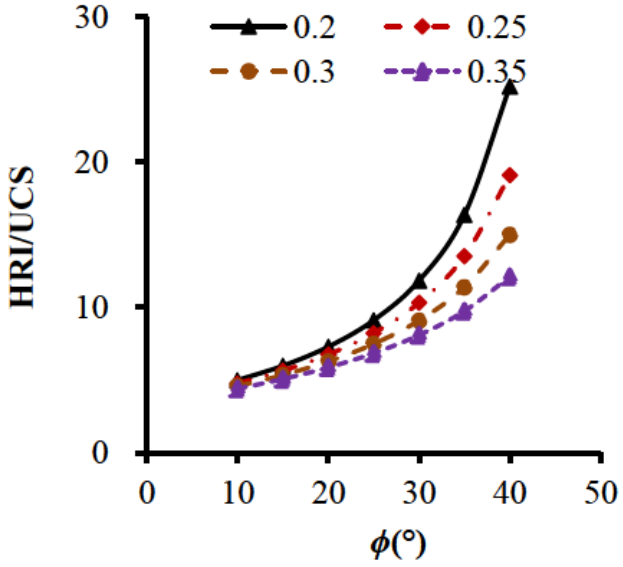

Figure 8b: Poisson's ratio effects on HRI/UCS in different angle of internal friction.

mainly in the range of −1.41%–8.92%, −5.91%–3.94% and −8.22%–13.22% respectively for siltstone, volcanic tuff, volcanic breccia, shale, sand stone and glutenite except mudstone. Observing the carters, it can be known that the mudstone exhibit "sink-in" and "cylinder" morphology and similar to the indenter after indention hardness test, while the others exhibit "cone". The phenomenon shows that the mudstone represents more ductility character than other specimens. In this situation, it is not satisfied the assumption of crushing process and M-C failure criterion, which results in a bigger percentage error. The errors except mudstone are considered excellent for the study of rock materials.

6 Conclusions

A theoretical study on the indentation process, the rock crushing mechanism and the relation between unconfined compressive strength (UCS) and indentation hardness (HRI) are carried out for brittle rock. Based on the stress distribution, indentation process and Mohr–Coulomb failure criterion, the mathematical mechanical equations are proposed to describe the depth and apex angle of craters, and the relation between UCS and HRI. The conclusions are as follows:

- The depth and apex angle of craters are all affected by the angle of internal friction and Poisson's ratio.

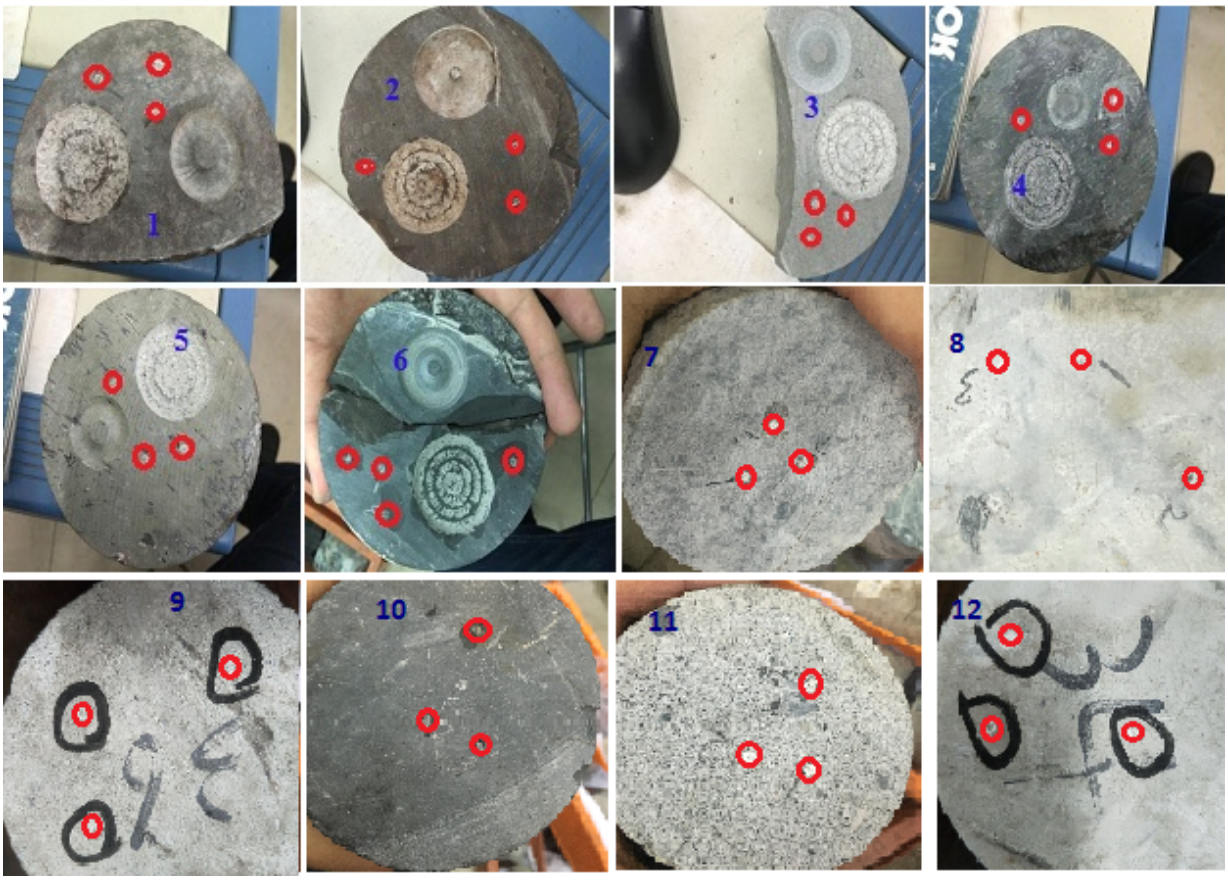

Figure 9: Rock specimens used in our tests.

- With the increase of the angle of internal friction, the depth of craters increase as exponential function, the apex angle of craters increase as linearity function, HRI/UCS ratio increases in an exponential function.
- With the increase of the Poisson ratio, the depth of craters increase as linearity function, the apex angle of craters decrease as linearity function, HRI/UCS ratio decreases as an exponential function
- The theoretic formulas including depth and apex angle of craters and HRI/UCS ratio are validated for most natural brittle rocks taken from Da Qing oilfield, the percentage error between the test and calculated results which are less than 10% for 90% samples.
- The proposed model is effective for predicting the shape of craters, the indentation hardness (HRI) or uniaxial compressive strength (UCS).

Acknowledgement: The research is supported by NSFC (Natural Science Foundation of China,No.51490650 and No. 51504067) and Postdoctoral foundation of Hei Long Jiang province (No.LBH-Z15031) and Young innovative talents of HeiLong Jiang province (UNPYSCT-2016123) in the context of northeast petroleum university.

References

[1] Tabor D., The physical meaning of indentation and scratch hardness. British Journal of Applied Physics, 2002, 7(5), 159.

[2] Sinha S. K., Reddy S. U., & Gupta M., Scratch hardness and mechanical property correlation for mg/sic and mg/sic/ti metal–matrix composites. Tribology International, 2006, 39(2), 184-189. DOI: 10.1016/j.triboint.2005.04.017.

[3] Kolek J., An appreciation of the schmidt rebound hammer. Magazine of Concrete Research, 1958, 35(2), 144-149.

[4] Selig E. T., Gunsallus K. L., Kulhawy F. H., & O'Rourke T. D., Evaluation of schmidt hammer rebound hardness test holders. Geotechnical Testing Journal, 1984, 7(3), 164-166. DOI: 10.1520/GTJ10493J.

[5] Kundu P. P., & Kukreja T. R., Surface modification of carbon black by vegetable oil—its effect on the rheometric, hardness, abrasion, rebound resilience, tensile, tear, and adhesion properties. Journal of Applied Polymer Science, 2010, 84(2), 256-260. DOI: 10.1002/app.10320.

[6] Hwang K. C., Huang Y., Li M., & Xue Z., The influence of indenter tip radius on the micro-indentation hardness. Journal of Engineering Materials & Technology, 2002, 124(3): 371-379.

[7] Kahraman S., Balcı C., Yazıcı S., & Bilgin N., Prediction of the penetration rate of rotary blast hole drills using a new drillability index. International Journal of Rock Mechanics & Mining Sciences, 200, 37(5), 729-743. DOI: 10.1016/S1365-1609(00)00007-1.

[8] Li D., Li S.J., YUS., Fractal characteristics of rock fragmentation process induced by indenters. Chinese Journal of Geotechnical Engineering,2013, 35(2), 314-319.

[9] Lu L.X., Mechanism on equivalent press-pole breaked for press-head to insert brittle rock in equilibrium. Journal of Xiangtan Mining Institute,2003, 18(1),13-16. DOI:10.3969/j.issn.1672-9102.2003.01.004

[10] Shi X., Tao Z., Meng Y., Li G., Zhang T., & Zhao X., The mechanism of rock breakage during bit-tooth penetration: a review. Geological Science & Technology Information, 2014, 33(4):225-230.

[11] Wijk G., The indenter test for rock drillability classification. Int. J. Rock Mech. Min. Sci. Geomech. Abstr., 1989, 26(1), 37–44

[12] Yu, Rules of rock fragmentation with mechanical methods and model of rock failures mechanism. Journal of china coal society, 1982, 3, 10-18.

[13] Cheatham, J. B. J., Rock-bit tooth friction analysis. Society of Petroleum Engineers Journal, 1963, 3(4), 327-332.

[14] Xia H.N., Wang K.X.,Zhai Y.H., Experimental research of PDC cutter shapes on breaking rock efficiency under various confining pressures" Journal of Jiang Han petroleum institute, 1997, 19(4), 48-50.

[15] Yang Y.X., Zhang W.W., Li B., Effect evaluation on insert penetration to rock and optimization of insert shape", Chinese Journal of Rock Mechanics and Engineering, 2001, 20(1), 110-113.

[16] Xu X.H., Rock fragmentation. Beijing: Coal Industry Press, 1984: 57-97.

[17] Zhang L., Cao P., & Radha K. C.,Evaluation of rock strength criteria for wellbore stability analysis. International Journal of Rock Mechanics & Mining Sciences,2010, 47(8), 1304-1316.

[18] Norbeck J. H., Mcclure M. W., Lo J. W., & Horne R. N., An embedded fracture modeling framework for simulation of hydraulic fracturing and shear stimulation. Computational Geosciences, 2016, 20(1): 1-18.

[19] Ma H., Yang C., Li Y., Shi X., Liu J., & Wang T., Stability evaluation of the underground gas storage in rock salts based on new partitions of the surrounding rock. Environmental Earth Sciences, 2015, 73(11), 6911-6925.

[20] ASTM. American Society for Testing and Materials. Standard test method for unconfined compressive strength of intact rock core specimens. ASTM D2938, 1984.

[21] Palchik V., Influence of porosity and elastic modulus on uniaxial compressive strength in soft brittle porous sandstones. Rock Mechanics & Rock Engineering, 1999, 32(4), 303-309.

[22] Liu J., Wang E., Song D., Wang S., & Niu Y., Effect of rock strength on failure mode and mechanical behavior of composite samples. Arabian Journal of Geosciences, 2015, 8(7), 4527-4539.

[23] Broch E. and Franklin J.A. The point-load strength test. Int J Rock Mech &Min Sci & Geomech Abstr , 1972, 9(6):669–697.

[24] Sheorey P.R., Barat D. and Das M.N., Schmidt hammer rebound data for estimation of large scale in situ coal strength. Int J Rock Mech &Mining Sci & Geomech Abstracts, 1984, 21:39–42.

[25] Sachpazis C.I., Correlating Schmidt hardness with compressive strength and Young's modulus of carbonate rocks. Bull EngGeol Environ ,1990, 42, 75–83.

[26] Tug˘rul A. and Zarif I.H., Correlation of mineralogical and textural characteristics with engineering properties of selected granitic rocks from Turkey. EngGeol, 1999, 51:303–317

[27] Shalabi F.I., Cording E.J. and Al-Hattamleh, O.H., Estimation of rock engineering properties using hardness tests. EngGeol, 2007, 90, 138–147.

[28] Wang H., Lin H. and Cao P., Correlation of ucs rating with schmidt hammer surface hardness for rock mass classification. Rock Mechanics & Rock Engineering, 2016, 50(1), 1-9.

[29] Wijk G., The indenter test for rock drillability classification. Int. J. Rock Mech. Min. Sci. Geomech.Abstr., 1989, 26(1), 37–44.

[30] Hertz H., On the contact of elastic solids. J.reine Angew.math, 1881, 92, 156. DOI:10.1103/PhysRevA.31.1957.3

[31] Riccardi B, Montanari R. Indentation of metals by a flat-ended cylindrical punch. Materials Science & Engineering A, 2004, 381(1):281-291.

[32] Boussinesq J., Application des potentiels à l'étude de l'équilibre et du mouvement des solides élastiques, principalement au calcul des déformations et des pressions que produisent, dans ces solides, des efforts quelconques exercés sur une petite partie de leur sur[J]. Revista Internacional De Lingüística Iberoamericana, 2008, 17(4), 105-118.

[33] Lindqvist P.A., Rock fragmentation by indentation and disc cutting : some theoretical and experimental studies. Biologia Plantarum, 1982, 35(1):107-112.

[34] Lindqvist P. A., Lai H. H., & Alm O., Indentation fracture development in rock continuously observed with a scanning electron microscope. International Journal of Rock Mechanics & Mining Sciences & Geomechanics Abstracts, 1984, 21(4), 165-182.

[35] Tan X. C., Kou S. Q., & Lindqvist P. A., Application of the ddm and fracture mechanics model on the simulation of rock breakage by mechanical tools. Engineering Geology, 1998, 49(3), 277-284.

[36] Hood M., Alehossein H., A development in rock cuttingtechnology. Int J Rock Mech Min Sci , 2000, 37:297–305

[37] Detournay E., Richard T., Shepherd M., Drilling response of dragbits: theory and experiment. Int J Rock Mech Min Sci, 2008, 45, 1347–1360.

[38] Wang S. Y., Sloan S. W., Liu H. Y., & Tang C. A., Numerical simulation of the rock fragmentation process induced by two drill bits subjected to static and dynamic (impact) loading. Rock Mechanics & Rock Engineering, 2011, 44(3), 317-332.

[39] Paul B., A modification of the coulomb-mohr theory of fracture. Journal of Applied Mechanics, 1961, 28(2), 259-268. DOI: 10.1115/1.3641665.

[40] Murrell S.A.F., A criterion for brittle fracture of rocks and concrete under triaxial stress, and the effect of pore pressure on the criterion. In: Fairhurst C. (Ed.), Proceedings of the 5th US symposium on rock mechanics, Minneapolis, 1963, 563–577.

[41] Andreev G. E., Brittle failure of rock materials:test results and constitutive models. A.A. Balkema, 1995, 33(2), 378.

[42] Al-Ajmi A.M., Zimmerman, R.W., Relation between the Mogiand the Coulomb failure criteria. Int J Rock Mech Min Sci, 2005, 42, 431–439.

[43] Singh M., Raj, A., & Singh, B., Modified mohr–coulomb criterion for non-linear triaxial and polyaxial strength of intact rocks. International Journal of Rock Mechanics & Mining Sciences, 2011, 48(4), 546-555.